

Objective rapid delineation of areas at risk from block-and-ash pyroclastic flows and surges

C. Widiwijayanti · B. Voight · D. Hidayat · S. P. Schilling

Received: 5 February 2008 / Accepted: 20 October 2008 / Published online: 29 November 2008
© Springer-Verlag 2008

Abstract Assessments of pyroclastic flow (PF) hazards are commonly based on mapping of PF and surge deposits and estimations of inundation limits, and/or computer models of varying degrees of sophistication. In volcanic crises a PF hazard map may be sorely needed, but limited time, exposures, or safety aspects may preclude fieldwork, and insufficient time or baseline data may be available for reliable dynamic simulations. We have developed a statistically constrained simulation model for *block-and-ash type PFs* to estimate potential areas of inundation by adapting methodology from Iverson et al. (Geol Soc America Bull 110:972–984, 1998) for lahars. The predictive equations for block-and-ash PFs are calibrated with data from several volcanoes and given by $A=(0.05 \text{ to } 0.1)V^{2/3}$, $B=(35 \text{ to } 40)V^{2/3}$, where A is cross-sectional area of inundation, B is planimetric area and V is deposit volume. The proportionality coefficients were obtained from regression analyses and comparison of simulations to mapped deposits. The method embeds the predictive equations in a GIS program coupled with DEM topography, using the *LAHARZ* program of Schilling (1998). Although the method is objective and reproducible, any PF hazard zone so computed should be considered as an approximate guide only, due to uncertainties on the coefficients applicable to individual PFs, the authenticity of DEM details, and the volume of future collapses. The statistical

uncertainty of the predictive equations, which imply a factor of two or more in predicting A or B for a specified V , is superposed on the uncertainty of forecasting V for the next PF to descend a particular valley. Multiple inundation zones, produced by simulations using a selected range of volumes, partly accommodate these uncertainties. The resulting maps show graphically that PF inundation potentials are highest nearest volcano sources and along valley thalwegs, and diminish with distance from source and lateral distance from thalweg. The model does not explicitly consider dynamic behavior, which can be important. Ash-cloud surge impact limits must be extended beyond PF hazard zones and we provide several approaches to do this. The method has been used to supply PF and surge hazard maps in two crises: Merapi 2006; and Montserrat 2006–2007.

Keywords Pyroclastic flow · Pyroclastic surge · Hazard maps · Volcano hazards · Montserrat · Merapi

Introduction

Pyroclastic flows and surges are arguably the most severe hazards from volcanoes, and appreciable efforts have been devoted to understanding these flowage processes and developing methods to aid the delineation of hazard zones. Assessments of pyroclastic flow hazards are often based on mapping of pyroclastic flow and surge deposits and estimations of inundation limits (Crandell et al. 1984), statistical relationships involving run-out distance (Calder et al. 1999) and/or computer models of varying degrees of sophistication (Denlinger and Iverson 2001; Patra et al. 2005; Esposti Ongaro et al. 2007, 2008). These methods are frequently limited. In the case of field studies, poor exposures or erosion may yield inadequate data in areas

Editorial responsibility: S. Nakada

C. Widiwijayanti · B. Voight (✉) · D. Hidayat
Department Geosciences, Penn State University,
University Park, PA 16802, USA
e-mail: voight@ems.psu.edu

B. Voight · S. P. Schilling
USGS Cascades Volcano Observatory,
1300 SE Cardinal Court, Suite 100,
Vancouver, WA 98683-9589, USA

of critical interest, and in the case of modeling, there inevitably are large uncertainties on rheologies and dynamic parameters. In many volcanic crises a hazard map for pyroclastic flows and surges is sorely needed, but limited time, exposures, or safety aspects may preclude field work, and insufficient computational time or baseline data may be available for adequately reliable dynamic simulations of future pyroclastic flow or surge events.

In this paper the term “flow” refers to a densely concentrated, avalanche-like stream of hot debris, and “surge” refers to the gravity-driven transport of hot ash in a relatively dilute and turbulent suspension (Calder et al. 1999). There are several types of pyroclastic flows and surges (Cas and Wright 1987), and here we focus on the block-and-ash type of pyroclastic flow caused by the collapse and disintegration of suitable lava dome material or lava flow fronts (Voight et al. 2000a, b; Calder et al. 2002), rather than on pyroclastic flows associated with fountain collapse. Such flows include those generated passively, during inactive periods or with slow dome growth, and actively generated collapses from rapidly growing portions of the dome or shear-lobe headwalls (Calder et al. 2002). We are also concerned with pyroclastic surges associated with, and commonly generated above pyroclastic flows, because such surges can decouple and extend beyond the limits of the PFs.

Here we describe development, testing, and implementation of an alternative method for delineating block-and-ash type pyroclastic flow (PF) hazard zones. We follow a procedure that had been developed previously to delineate lahar-inundation hazard zones (Iverson et al. 1998). The method is rapid, objective, and reproducible, can be used to supplement traditional or modeling methods, or used where data, time, or personnel are inadequate for the application of traditional field or modeling methods. We also consider several approaches to estimate the potential influence of ash-cloud surges.

Following the approach of Iverson et al. (1998), we have developed a statistically constrained simulation model for block-and-ash PFs calibrated with data from many volcanoes to estimate potential areas of PF inundation. The method uses statistical data and scaling to develop semi-empirical equations that predict the valley cross-sectional area (A) and planimetric area (B) inundated by block-and-ash PFs with various volumes (V). The planimetric area is simply the deposit map area, and the cross-section area embodies the lateral limits and average thickness of the valley inundation as measured normal to the thalweg (Iverson et al. 1998, Fig. 1). Scaling analyses as developed by Iverson et al. (1998) provide a rationale for using proportionality rules $A \propto V^{2/3}$, and $B \propto V^{2/3}$. The data and statistics test the validity of these rules as applied to PFs, and yield the values of proportionality coefficients. The calibrated predictive equa-

tions for block-and-ash PF inundation are given by $A=(0.05$ to $0.1) V^{2/3}$, $B=(35$ to $40) V^{2/3}$, and these provide all the information necessary to plot PF inundation limits on a topographic base.

The method embeds predictive equations in a GIS (geographic information system) program coupled with DEM (digital elevation model) topography, using the *LAHARZ* program of Schilling (1998). The approach enables delineation of overlapping inundation zones for a selection of PF volumes, yielding an automated display of gradations in hazard. The model does not explicitly consider dynamics aspects, which can be an important limitation. Pyroclastic surge impacts must be extended beyond PF hazard zones and we explore several approaches to do this. The method has been used to quickly supply PF hazard maps in two recent volcano crises: Merapi 2006; and Montserrat 2006–2007. We also have compared our *PFz maps* (using the term coined by C. Newhall; 2006, “personal communication”) to recent PFs that were deposited after the maps were produced, and to maps generated by several other model techniques.

Statistical basis and data attributes

To test the proportionality rules and calibrate the governing equations, we analyze trends for pyroclastic flows of the block-and-ash type. Testing involves statistical determination of whether the cross-sectional and planimetric areas A and B are approximately proportional to $V^{2/3}$, as scaling suggests. Calibration involves determining statistically-based values of the proportionality coefficients.

The equations are in power law form and can be linearized by logarithmic transformation (Iverson et al. 1998), yielding

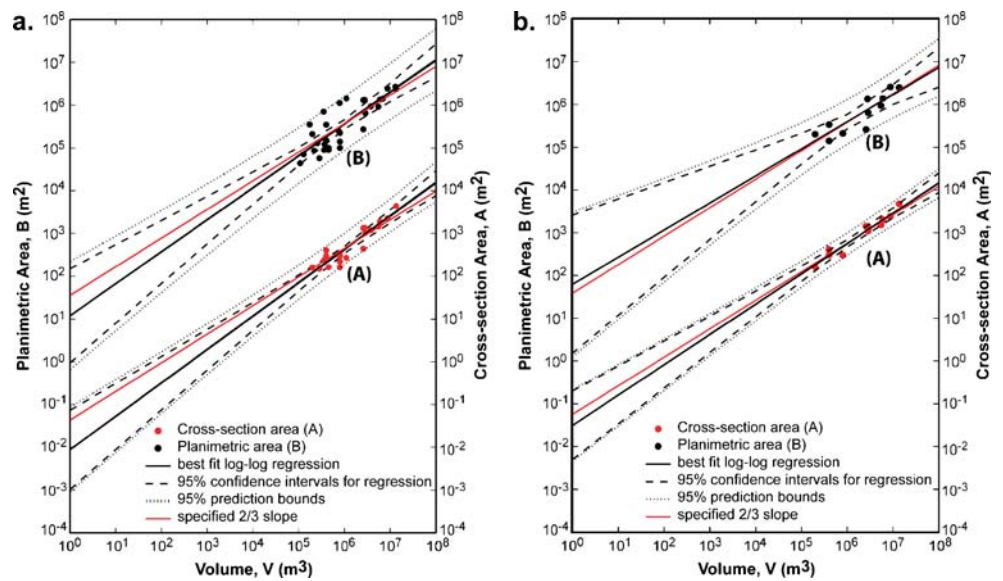
$$\log A = \log C + (2/3) \log V \quad (1)$$

$$\log B = \log c + (2/3) \log V \quad (2)$$

where $2/3$ is the slope and $\log C$ and $\log c$ are the A and B intercepts, respectively, on log–log plots (the values of $\log A$ and $\log B$, respectively, where $\log V$ equals zero). These equations constitute null hypotheses, providing a model that can be rejected if the real relations between $\log A$ or $\log B$ and $\log V$ are non-linear or have a slope significantly different from $2/3$ (Iverson et al. 1998).

The data we used are based on historical flows and are summarized in Table 1. The PF volumes in Table 1 are estimates of the single value most representative of the volume of a given PF as it enters the depositional area. Multiple volume estimates are not used in order to avoid the associated statistical bias. In general we estimate the

Fig. 1 Scatter plots of inundated valley cross-section area A and planimetric area B as a function of PF volume V , using the data of Table 1. The best fit log–log regression lines and 95% confidence intervals for regression, and prediction, are also shown. Red lines show the trend for specified 2/3 slope. **a** Data from Table 1. **b** Montserrat data only



maximum instantaneous flow volume, determined from deposited sediment volumes. In some cases we made calculations to determine planimetric and valley cross-section areas, and in other cases the literature was used, as indicated in table notes. The inundation areas represented are referenced mainly to depositional areas on lower slopes, and not to proximal regions on the steeper volcano flanks which may also contain some, and usually thin, deposits. This usage is consistent with the application of the method, which aims to predict inundation beyond the proximal hazard zone. The data in Table 1 are rounded to, at most, three significant figures. Higher apparent precision is noted in much literature data, but our impression is that the accuracy of calculations are seldom greater than this. Our use of log-transformed data in statistical analyses accommodates the variation in precision and data accuracy.

Data for large flows is limited, say $V > 1.5 \times 10^7$ m³. Events of larger size are fairly exceptional but have occurred for instance on Montserrat (to $\sim 20 \times 10^7$ m³, the largest historical dome collapse worldwide). In the Montserrat cases the run-out extended offshore and subaerial inundation data are lacking or irrelevant. No doubt good data for large PFs will be found, but for the moment the database is limited with respect to large flows, and prediction of PF inundation areas of large flows may involve an extrapolation. Likewise we lack data for small flows, say $V < 10^5$ m³. Small PFs are possible but volcanic flows of this scale are commonly characterized as rockfalls, have shorter run-outs, are less hazardous, elutriate less fines, and may exhibit different mobilities and inundation properties in comparison to PFs. Thus the absence of data in this class avoids bias in relation to the properties of PF events more likely to reach down-valley populated areas.

For most events, we have data for both the typical valley cross section area inundated and the planimetric area

inundated (deposit area), but for some we lack data on valley cross-section area. This does not affect statistical analysis because we treat the data as independent sets.

Statistical analyses

Table 2 and Fig. 1 give the results of statistical analyses, developed for two sets of data—the complete dataset, and a sub-set of eleven events from Montserrat. First, for all data, Fig. 1a shows data scatter and least-squares best fit regressions for both log A and log B , as a function of log V . The regression lines are bounded by 95% confidence-interval curves derived from t -distribution statistics. The curves enclose the region in which specification of log V enables the future values of log A or log B to be predicted with 95% confidence.

Following Iverson et al. (1998), we also develop the null hypothesis that asserts that the dependence of log A and log B on log V can be represented by lines with slopes of 2/3, as implied by scaling. A summary of the tests of the “2/3 slope” null hypothesis is given by the F statistic in Table 2, and the small value of these F statistics (compared to tabulated values of F distribution) indicates we cannot reject the null hypothesis that the differences between the linear “best-fit” models with slopes of 0.779 and 0.741, and “2/3 slope” models, are not large. This conclusion is supported by the similarity of r^2 statistics for the “best-fit” and “2/3 slope” regressions in Table 2. Likewise on Fig. 1a, the lines described by the “2/3 slope” models generally fall well within the 95% confidence intervals for the regression lines. However, for volumes much in excess of the database range, say $> 10^8$ m³, the log A lines display some mismatch. Most of the data were acquired from literature and the data quality is likely mixed but difficult to assess.

Table 1 Pyroclastic flow deposit data

Code of events	Name of events/location	Time of events	Reference/source of data	Flow volume, V (m ³) ^b	Cross-section area, A (m ²) ^c	Planimetric area, B (m ²) ^b	
1	SHV1 ^a	Mosquito Ghaut	3-Apr-96	Calder et al. (2002); Cole et al. (2002)	200,000	160	212,000
2	SHV2 ^a	Tar River Valley	12-May-96	Calder et al. (2002); Cole et al. (2002)	400,000	410	350,000
3	SHV3 ^a	Tar River Valley	29-Jul-96	Calder et al. (2002); Cole et al. (2002)	2,800,000	1,350	1,320,000
4	SHV4 ^a	White River	30-Mar-97	Calder et al. (2002); Cole et al. (2002)	2,600,000	1,340	272,000
5	SHV5 ^a	White River	11-Apr-97	Calder et al. (2002); Cole et al. (2002)	2,900,000	1,050	648,000
6	SHV6 ^a	Tuitt's Ghaut	5-Jun-97	Calder et al. (2002); Cole et al. (2002)	400,000	300	152,000
7	SHV7 ^a	Mosquito Ghaut	17-Jun-97	Calder et al. (2002); Cole et al. (2002)	800,000	300	223,000
8	SHV8 ^a	Mosquito Ghaut	25-Jun-97	Calder et al. (2002); Cole et al. (2002)	5,500,000	1,440	920,000
9	SHV9 ^a	Fort Ghaut/Gages Valley	3-Aug-97	Calder et al. (2002); Cole et al. (2002)	8,800,000	2,240	2,460,000
10	SHV10 ^a	Mosquito & Tuitt's Ghauts	21-Sep-97	Calder et al. (2002); Cole et al. (2002)	13,600,000	4,350	2,400,000
11	SHV11 ^a	White River	6-Nov-97	Calder et al. (2002); Cole et al. (2002)	6,000,000	1,880	1,340,000
12	Mer1	Kali Sat 2	1998	Schwarzkopf and Schmincke (2000)	258,000	N.D.	129,000
13	Mer2	Kali Senowo 2 & 3	1998	Schwarzkopf and Schmincke (2000)	285,000	150	57,000
14	Mer3	Kali Lamat	1998	Schwarzkopf and Schmincke (2000)	109,000	N.D.	43,800
15	Mer4	Kali Putih/Sat North I	1998	Schwarzkopf and Schmincke (2000)	21,900	N.D.	87,500
16	Mer5	Kali Putih/Sat North II	1998	Schwarzkopf and Schmincke (2000)	175,000	N.D.	350,000
17	Mer6	Kali Putih/Sat South I	1998	Schwarzkopf and Schmincke (2000)	368,000	N.D.	123,000
18	Mer7	Kali Putih/Sat South II	1998	Schwarzkopf and Schmincke (2000)	350,000	N.D.	700,000
19	Mer9 ^a	Kali Boyong	22-Nov-94	Abdurachman et al. (2000)	2,600,000	440	1,310,000
20	Col1	Colima 1991	1991	Saucedo et al. (2004, 2005)	800,000	160	100,000
21	Col2	Colima 1994	1994	Saucedo et al. (2005)	450,000	N.D.	100,000
22	Col3	Cordoban West	1998	Saucedo et al. (2002, 2005)	800,000	220	140,000
23	Col4	Cordoban East	1998	Saucedo et al. (2002, 2005)	450,000	160	90,000
24	Col5	Montegrande-San Antonio	1999	Saucedo et al. (2002, 2005)	790,000	340	230,000
25	Col6	La Lumbre	1999	Saucedo et al. (2002, 2005)	360,000	240	90,000
26	Col7	Phase I 1913	1913	Saucedo et al. (2005)	130,000	N.D.	70,000
27	Unz1 ^a	Mizunashi River	3-Jun-91	Nakada and Fujii (1993); Yamamoto et al. (1993)	789,000	320	1,110,000
28	Unz2 ^a	Mizunashi River	8-Jun-91	Nakada and Fujii (1993)	1,110,000	270	1,420,000
29	Unz3 ^a	Oshigadani River	15-Sep-91	Fujii and Nakada (1999)	3,800,000	1,190	927,000

N.D. no data

^a Cross-section and planimetric areas were obtained by CW and BV from digitized deposit maps superimposed on DEMs

^b The numbers are rounded to maximum of three significant figures

^c The cross section areas are rounded to the nearest 10 m²

Similar results are shown for the high quality Montserrat dataset in Table 2 and Fig. 1b. In this case the differences between linear “best-fit” models (with slopes of 0.707 and 0.634) and “2/3” slope models are very small. The r^2 statistics are very similar for the two models (and higher than for the complete dataset), and the graphical plots show a very close match of lines for the two models, even when extrapolated far beyond the data range.

For practical use we adopt the “2/3 slope” model, and we suggest rounded-off parameter values as follows:

$$\text{For all data: } A=0.05 V^{2/3}, B=35 V^{2/3}$$

$$\text{For Montserrat data: } A=0.1 V^{2/3}, B=40 V^{2/3}$$

The statistical uncertainty of these equations is measured approximately by the standard errors listed in Table 2, which imply an uncertainty of a factor of about

two or more in predicting A or B for a specified V . The statistical values reported in Table 2 for least-squares fits using the “2/3 slope” model differ slightly from those developed with stipulated rounded-off intercepts (not shown). However before accepting such values, we tested the predicted inundations against mapped PFs, as discussed below.

Implementation

Implementation does not require use of GIS, but GIS surely facilitates it and we have used the LAHARZ programs developed to perform the task. LAHARZ is a suite of Arc/INFO macrolanguage (AML) programs that run within the cell-based Grid Program of Arc/INFO (Schilling 1998). Model input consists of a DEM of topography, derived

Table 2 Parameters and analysis-of-variance statistics for models of log-transformed PF data

	Best-fit regression	Slope=2/3	Zero slope
PF events			
<i>Model for prediction of cross-section area, A</i>			
Slope of line	0.779	0.667	0
Intercept of line at log $V=0$	-2.060	-1.372	2.713
Number of data pairs (N)	21	21	21
Residual degrees of freedom (DF)	19	20	20
Summed square of residuals (SS)	0.545	0.616	3.924
Residual mean square (MS)	0.029	0.031	0.196
Coefficient of determination (r^2)	0.861	0.843	0
Standard error of model (σ)	0.169	0.175	0.443
F statistic (comparison to best-fit regression)	N.A.	2.475	117.8
<i>Model for prediction of planimetric area, B</i>			
Slope of line	0.741	0.667	0
Intercept of line at log $V=0$	1.100	1.541	5.486
Number of data pairs (N)	29	29	29
Residual degrees of freedom (DF)	27	28	28
Summed square of residuals (SS)	2.748	2.800	7.845
Residual mean square (MS)	0.102	0.099	0.280
Coefficient of determination (r^2)	0.650	0.643	0
Standard error of model (σ)	0.319	0.316	0.529
F statistic (comparison to best-fit regression)	N.A.	0.511	50.079
Montserrat PFs data			
<i>Model for prediction of cross-section area, A</i>			
Slope of line	0.707	0.667	0
Intercept of line at log $V=0$	-1.515	-1.253	2.951
Number of data pairs (N)	11	11	11
Residual degrees of freedom (DF)	9	10	10
Summed square of residuals (SS)	0.105	0.112	1.975
Residual mean square (MS)	0.012	0.011	0.197
Coefficient of determination (r^2)	0.947	0.943	0
Standard error of model (σ)	0.108	0.106	0.444
F statistic (comparison to best-fit regression)	N.A.	0.6	160.286
<i>Model for prediction of planimetric area, B</i>			
Slope of line	0.634	0.667	0
Intercept of line at log $V=0$	1.786	1.582	5.784
Number of data pairs (N)	11	11	11
Residual degrees of freedom (DF)	9	10	10
Summed square of residuals (SS)	0.428	0.432	1.927
Residual mean square (MS)	0.048	0.043	0.193
Coefficient of determination (r^2)	0.778	0.776	0
Standard error of model (σ)	0.218	0.208	0.439
F statistic (comparison to best-fit regression)	N.A.	0.084	31.521

N.A. not applicable

supplementary grids, specified flow volumes, and a user-specified upstream limit to the inundation boundary. LAHARZ calculates the inundated valley cross-sectional area (A), identifies planimetric grid areas contributed by successive downstream cross-sections, calculates the cumulative planimetric areas, and stops the calculation when cumulative planimetric area equals the total inundation area defined by B .

In general for practical use in hazards assessment, we used the program to predict and map a range of PF inundation areas for a specified range of V , and in this way to display a gradation of hazard. Then the statistical uncertainty of the predictive equations, as estimated by the standard errors in Table 2, is superposed on the uncertainty of forecasting V for the next PF to descend a valley area. This is the conventional approach as followed

by Iverson et al. (1998), Major et al. (2004) and others, in presenting maps intended for use in hazards zonation. We follow a similar procedure to compare modeled inundations to historical PFs.

Results

We have tested and applied the technology to block-and-ash PF hazards at several volcanoes, notably Soufrière Hills volcano on Montserrat, and Merapi volcano in Java. Hazards from PFs are serious at both volcanoes, many previous events have been thoroughly documented (Calder et al. 1999, 2002; Voight et al. 2000a, b), and these locations are ideal for comparing our automated PF inundation predictions with real deposits and predictions from other methods.

Figure 2a shows the computed PF-inundation limits for areas surrounding Soufrière Hills volcano, Montserrat, intended for comparison with selected PF events. The rounded-off regression parameters used were based on the Montserrat data subset. Note that this is *not* a hazards map proposed to deal with future events, but simply a map of inundation limits which can be compared with some previous PF events of a given size. The nested color bands in different drainages involve different sets of prescribed flow volumes, for comparison with these selected events. To construct the mapped inundation zones, we used four reference volumes within each drainage, intending to bracket the volumes of specific flow events in those drainages. In Tar River Valley (map location 1), for instance, volume range is $0.4\text{--}5 \times 10^6 \text{ m}^3$, intended for comparison with relatively small PF events between April and August 1996 with estimated volumes between 0.2 and $4 \times 10^6 \text{ m}^3$ (Cole et al. 2002, Table 2, Fig. 2). In Mosquito Ghaut (location 2), the volume range is $0.8\text{--}10 \times 10^6 \text{ m}^3$, to bracket the event of 25 June 1997 with total PF volume about $5.5 \times 10^6 \text{ m}^3$ (Calder et al. 1999, 2002). In Tuitt's Ghaut (location 3) and White's Ghaut (location 4), the volume ranges are $1\text{--}14 \times 10^6 \text{ m}^3$, and $0.25\text{--}2 \times 10^6 \text{ m}^3$, respectively, for comparison with the event of 21 September 1997 with PF volume of $\sim 14 \times 10^6 \text{ m}^3$ (Calder et al. 2002), split between the two drainages. In Fig. 2a the Tuitt's and Mosquito drainages join up, so that the downvalley map pattern shown is dominated by the larger volumes from Tuitt's Ghaut; we treat the 25 June 1997 event in Mosquito separately in Fig. 3b. In Fort Ghaut (location 5), the volume range is $1\text{--}8.8 \times 10^6 \text{ m}^3$, with the larger value corresponding to the PF of 3 August 1997 (Calder et al. 2002). In White River (location 6), the reference volume range is $0.75\text{--}5 \times 10^6 \text{ m}^3$, for comparison to several events in March, April, and November 1997, with a volume range $1\text{--}6 \times 10^6 \text{ m}^3$ (Calder et al. 2002).

We specified the depositional starting points for our mapping by selecting a specific contour line across the drainage, often noted by a marked break in slope that experience had shown to demarcate the approximate boundary of upstream erosion and/or thin deposition, and thicker deposition downstream. The contour line selected could differ in different drainages. We suggest that for applications elsewhere, reasonable judgments can commonly be made based on examination of local topography, and if necessary, sensitivity runs can be made to ascertain the degree to which the choice of starting point affects runout. Different choices of starting point would shift the downstream limits of computed inundation zones, but would not affect the lateral limits of these zones (Iverson et al. 1998). In this respect the methodology is robust with respect to uncertainty about starting points. Other approaches have been used to define the starting position, such as the H/L (height/runout) energy-cone approach of Malin and Sheridan (1982) used by Iverson et al. (1998) for their lahar modeling studies. We do not use this method to define the limits of the "proximal zone", as it would give inconsistent starting point positions for the various drainages in relation to topography. It is by itself a method to estimate the runout of pyroclastic flows, but we consider its physical basis suspect, inasmuch as it ignores the mass of the flow.

We used the 1996 Montserrat island DEM at 10 m resolution to represent our computational grid. Even for historical PF events confined in a narrow channel, this resolution is sufficient to represent the areas inundated. To simulate the most recent PF hazard into Belham River drainage (Fig. 4) we used a DEM updated to November 2006 (R. Herd, unpublished data; G. Wadge, unpublished data).

For reference, Fig. 2b depicts topography and the principal block-and-ash flow and associated surge deposits formed between 1996 and 1999 (Cole et al. 2002), but there are some important differences between this map and Fig. 2a that need to be noted, as a precise match of patterns on the two maps is not to be expected. First, Fig. 2b contains patterns for additional events, not considered in our analysis, which greatly broaden some of the map patterns: e.g. for Tar River, where the entire valley floor was covered by larger events such as the $20\text{--}25 \times 10^6 \text{ m}^3$ collapse of 3 July 1998 (Norton et al. 2002), and the White River and surrounding region, affected by the "directed volcanic blast" of 26 December 1997 with volume $>25 \times 10^6 \text{ m}^3$ (Sparks et al. 2002; Esposti Ongaro et al. 2008). Second, the map of Fig. 2b also includes pyroclastic surge deposits, which expand the area mapped for several events (25 June 1997, 3 August 1997, 21 September 1997) but are not explicitly predicted by the PF simulation model. However, we discuss the pyroclastic surge question below and suggest procedures to include it in the hazard map strategy.

Fig. 2 a Block-and-ash PF inundation simulations for Montserrat, using $A=0.1 V^{2/3}$, $B=40 V^{2/3}$. Volume ranges specified for each drainage are indicated in the inset table. Surge limits are not simulated. **b** Principal block-and-ash PF deposits on Montserrat formed between 1996 and 1999 (after Cole et al. 2002). Deposit areas include associated surge or volcanic blast deposits

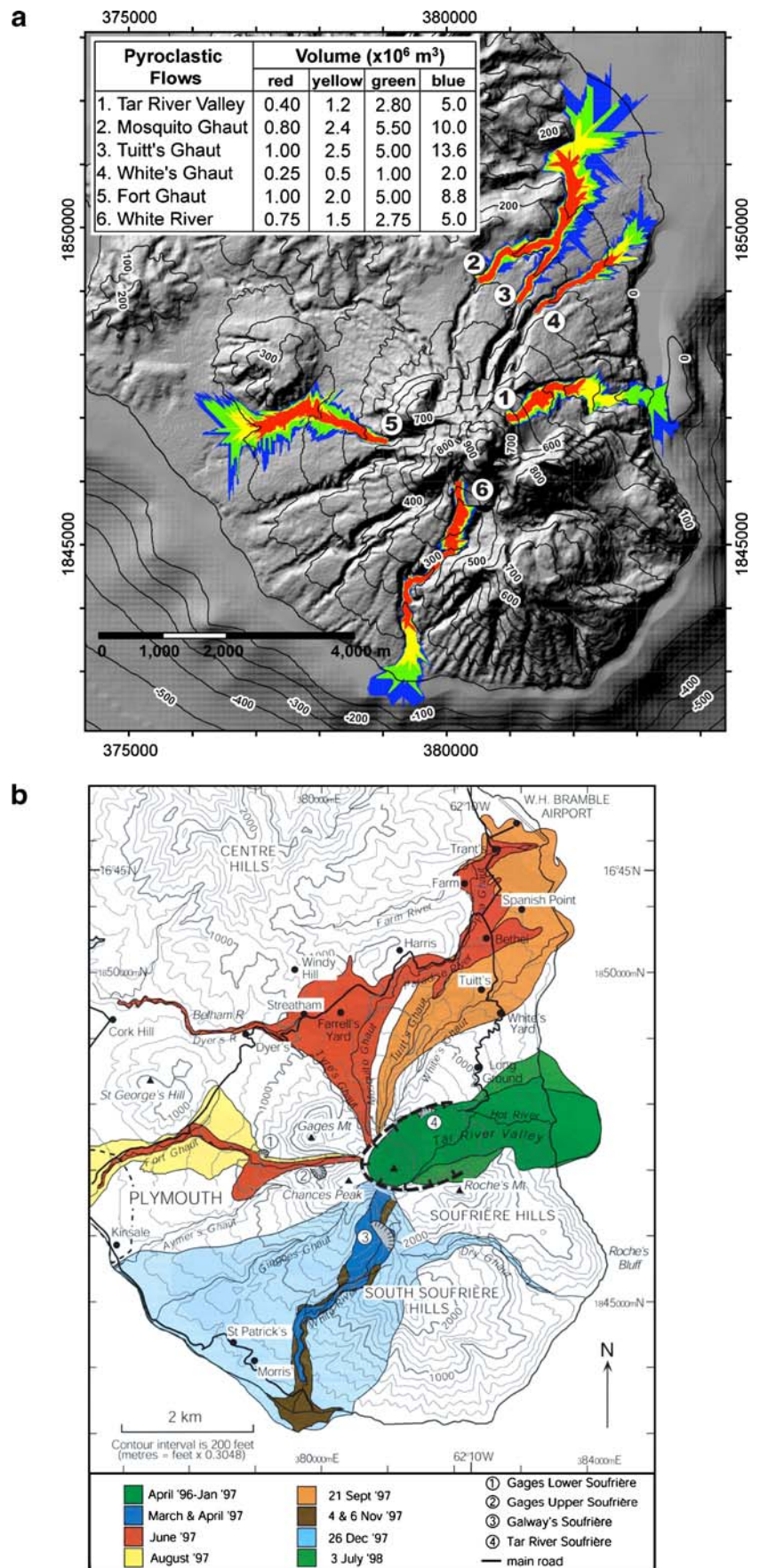


Fig. 3 **a** Map showing extent of 25 June 1997 block-and-ash PF deposit, Montserrat, and associated surge deposits (after Loughlin et al. 2002a). **b** Simulations of block-and-ash PF inundations for the topography of 25 June 1997 using $A=0.1 V^{2/3}$, $B=40 V^{2/3}$ and selected volumes. Surge limits are not simulated

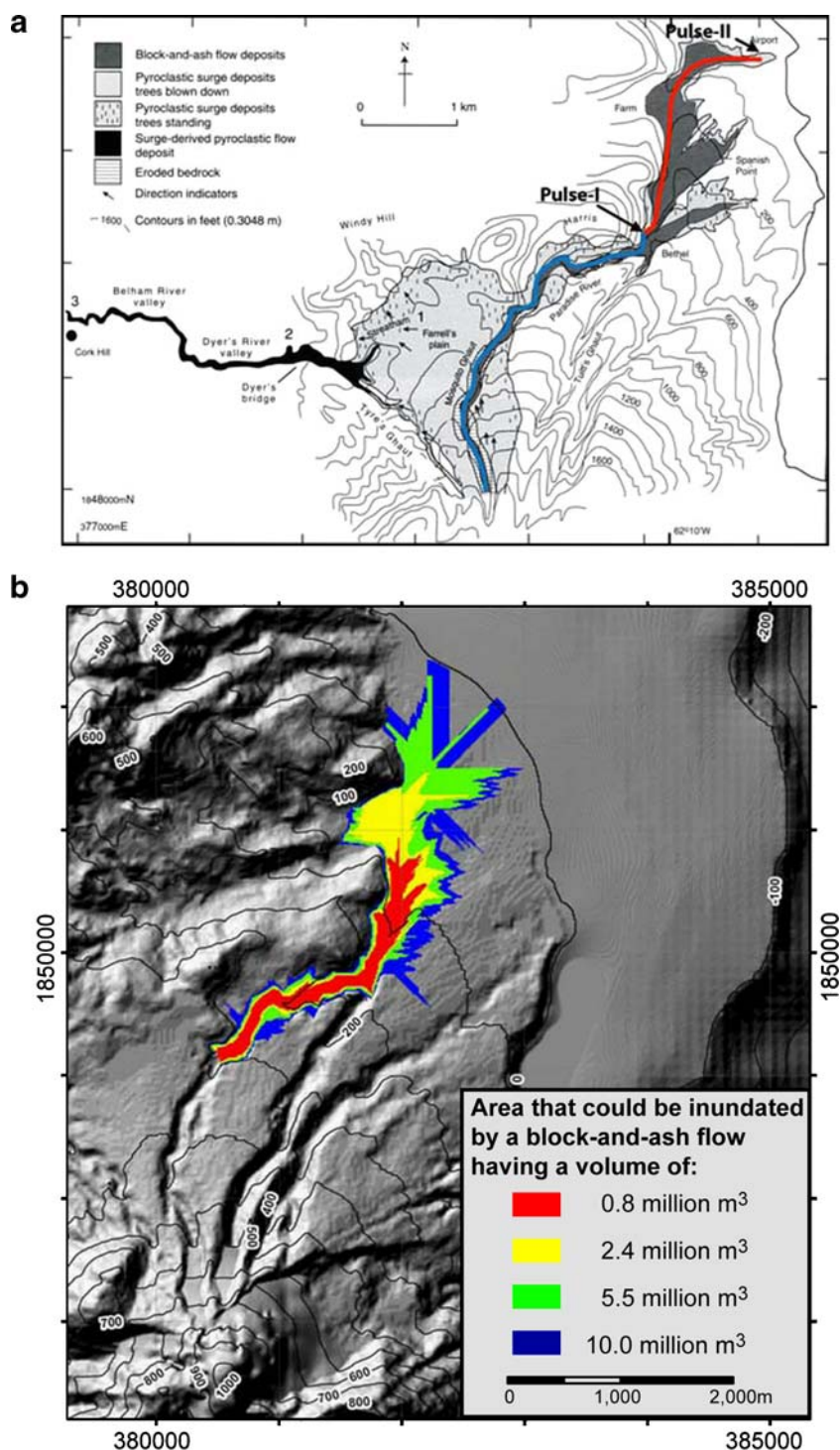
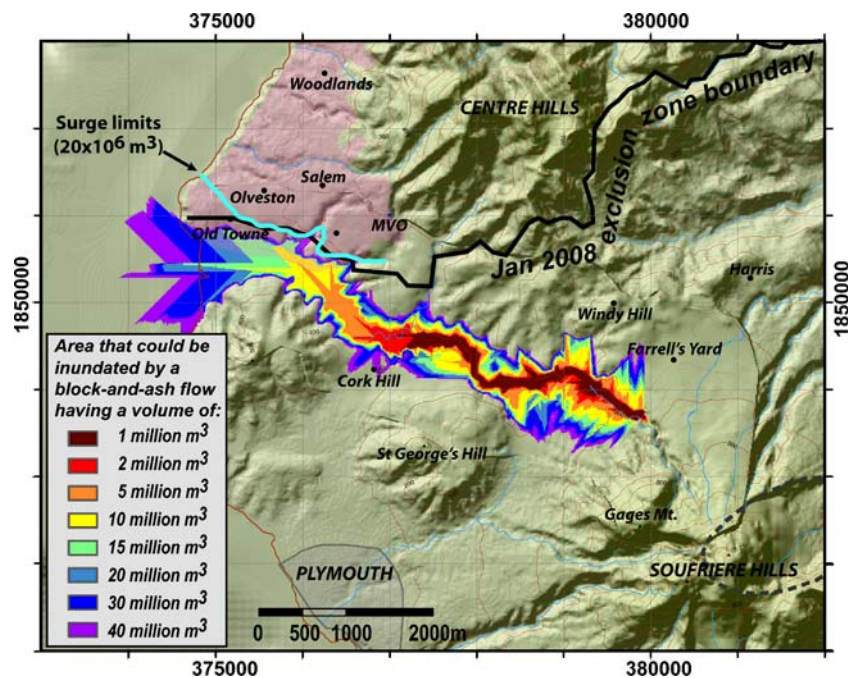


Figure 3b illustrates details of the computed inundation zones for flows originating in Mosquito Ghaut, for comparison with the mapped PF of 25 June 1997 (Fig. 3a; Loughlin et al. 2002a, b). This was a watershed event in the history of Montserrat, with 19 persons killed and enormous socio-economic and political consequences (Kokelaar 2002). Using the parameters $A=0.1 V^{2/3}$, $B=40 V^{2/3}$, the map shows nested inundation zones calculated

for volumes of 0.8, 2.4, 5.5, and $10 \times 10^6 \text{ m}^3$. The actual 25 June event involved $5.5 \times 10^6 \text{ m}^3$ in the PF, with an additional $0.9 \times 10^6 \text{ m}^3$ split off to form a pyroclastic surge (Calder et al. 1999). Most of the surge volume jumped the channel in the proximal zone and was unrelated to downstream PF dynamics (Fig. 3a). The model inundation zones attempt to assess the PF only. The actual PF lasted over 20 min and was characterized by three main pulses in

Fig. 4 Simulated inundations of block-and-ash PFs of selected volume for the Belham River drainage, Montserrat, to aid risk assessment in the volcanic crisis of Jan–Feb 2007. Parameters used are, $A=0.1 V^{2/3}$, $B=40 V^{2/3}$. Surge limit using the method of Wadge et al. (1998) shown by *pale blue line* for an assumed PF volume of $20 \times 10^6 \text{ m}^3$. Base topography updated to November 2006. Populated area shown in *pink*. January 2007 exclusion zone boundary shown by *black line*



rapid succession roughly estimated to comprise volumes of 0.8, 2.4, and $2.4 \times 10^6 \text{ m}^3$ (Loughlin et al. 2002a). Deposits of PF pulses one and two partially filled the main drainage channel so that the material of the third pulse spilled out of the channel in several places, inundating several small villages on the eastern coastal plain. Comparison of the maps suggests that overall, a very reasonable match is obtained by the model inundations in relation to the observed event, testing the parameters $A=0.1 V^{2/3}$, $B=40 V^{2/3}$. The green pattern for $5.5 \times 10^6 \text{ m}^3$ in Fig. 3b compares well with the dark grey area for deposits of the same cumulative volume in Fig. 3a. The differences in detail in the distal area largely reflect minor differences in real vs. idealized topography, and the irregular, “ragged” edges reflect grid-cell computational aspects and our preference (in this instance) to perform no smoothing. For the smaller pulses, the deposit of the actual $\sim 0.8 \times 10^6 \text{ m}^3$ pulse is slightly shorter than the modeled inundation zone of the same volume, and the $\sim 2.4 \times 10^6 \text{ m}^3$ pulse has a farther runout due to containment in the channel. But the differences appear in the details and we believe that the fit is acceptable generally, and is supportive of the methodology.

Similar comparisons between model and equivalent field data were made for all the drainages, but space here does not allow discussion in detail nor display of detailed field maps. We comment briefly on the other model inundation zones of Fig. 2a. With respect to Tar River (location 1), the inundation zones shown are reasonably well matched by field data. The 12 May 1996 PF, with volume $0.4 \times 10^6 \text{ m}^3$, is similar to the red zone of Fig. 2a with the same volume,

excepting a farther reaching tongue of the deposit in a narrow, deep channel (Cole et al. 2002, Fig. 2). The 29–31 July 1996 event, with $4 \times 10^6 \text{ m}^3$, reached the sea, similar to the green pattern on Fig. 2a. We note that in detail, each successive event modifies the topography, so that true tests of field versus models must use updated topography. This was done in the case of the PF of 21 September 1997 (location 3), which initiated in Tuit’s Ghaut, but with downstream topography modified by previous deposition on 25 June 1997. The resulting inundation map is shown on Fig. 2a, and compares well enough to deposits along the Tuit’s Ghaut and downstream drainage, and with overspill of one or two million m^3 into White’s Ghaut (location 4). The comparison map of Fig. 2b does not precisely show the NW margin of the 21 September PF deposits, but it does show Tuit’s Ghaut, Whites Ghaut, and the pyroclastic surge deposits that extend over and between the two drainages. A more detailed deposit map is given by Cole et al. (2002, Fig. 6). The resulting match of model inundation boundaries with deposit maps compares very well apart from minor details that largely reflect DEM precision. The Fort Ghaut (location 5) mapping slightly underestimates runout of the large PF of 3 August 1997, perhaps because of volume loss to lateral deposits, with small downstream definition of the channel. The deposit map pattern in yellow (Fig. 2b) includes pyroclastic surge deposits against the east side of St. Georges Hill, which of course are not treated by the PF model inundation maps. Finally, the White River model inundation zones (location 6) can be compared to several events in March and April 1997, each with a volume about $3 \times 10^6 \text{ m}^3$, and the 6

November 1997 PF, twice as large. The latter is matched approximately by the blue zone, $5 \times 10^6 \text{ m}^3$, which extends into the sea. The yellow zone, $2 \times 10^6 \text{ m}^3$, slightly exceeds runouts of the March and April PFs.

The inundation maps were based mostly on pre-eruption topography, and it will be appreciated that with each “major” PF or lahar event, deposition could change topography and influence future flows. The comparative test of mapped deposits versus calculated PF inundations in non-proximal areas shows that in most cases the fits are good. In some cases the model zones extended somewhat farther than deposits, and other cases somewhat less, but considering the variety in channel slopes and characteristics, and the degree of scatter in the A , B statistical plots, we conclude that the PF inundation zone methodology provided acceptable results. This test was applied to the data regression using the A coefficient of 0.1, and not to the “all data” regression, which differs mainly in the A statistic.

Accordingly, we have applied the method to real hazards assessments on Montserrat since Spring 2006. In early 2007 a main concern was the hazard produced by the recent changes in the size and direction of the growth of the lava dome, which had increased the risk toward the western sector. An example map (constructed February 2007) is shown in Fig. 4, giving inundation zones for major PFs that potentially could reach populated areas. The map was created using an upgraded DEM that took into account the latest channel changes (unpublished data from R. Herd and G. Wadge). A sharp break in slope of the drainage channel near the foot of Gages Mountain was used as the start point for deposition. These mapped inundation zones could have been truncated at the shoreline, but we did not alter them because they demonstrated (even if only roughly) that the actual hazard extended offshore. This was considered useful qualitative information in the deliberations on Montserrat about maritime hazard zonation. After this map was produced, a block-and-ash flow with a volume of about 2 Mm^3 occurred that well matched the inundation map. However, to allow conservatively for parameter uncertainty, we also developed a map using 0.05 as the parameter for the A calculation, based on the regression of the full dataset; this map yielded longer runout for a given volume. These maps were used by the Risk Assessment Panel, in concert with maps developed by other dynamic modeling approaches, such as the (essentially 1D) *PYRO-FLOW* approach (Wadge et al. 1998), *TITAN2D* (Patra et al. 2005; Widiwijayanti et al. 2004, 2006), and the 3D code *PDAC*, with the latter used to model a potential volcanic blast (Esposti Ongaro et al. 2008). This comparison proved useful, because our semi-empirical data-based results were more robust than were the dynamic models, with the latter very sensitive to dynamic parameters that were poorly constrained for large PF events. Our PF inundation maps

thus enabled the dynamic models to be used more effectively, by guiding choices on their parameters.

Similarly, we prepared inundation maps for Merapi volcano, to aid risk assessment in the volcanic crisis of May–July 2006 (Fig. 5). In May 2006, after 5 years of quiescence, activity at Merapi resumed with lava dome growth and associated block-and-ash flows directed mainly to the southwest sector. After the catastrophic M 6.3 Bantul earthquake on 27 May, activity peaked when a shift in the direction of dome growth, an increase of extrusion flux, and a breach of the southern rim enabled PFs to travel down the south and southeast flanks (C. Newhall, “written communications” to BV, June 2006; Ratdomopurbo 2007; Gertisser and Charbonnier 2007), affecting a region that had been free of such hazards for many decades (Voight et al. 2000a). We simulated flows for all the southern drainages but particular attention was given to Gendol River area. We used the parameters, $A=0.05 V^{2/3}$, $B=35 V^{2/3}$. PF hazard zones were graded from high to low (and expressed in our communications in the Indonesian language), which represented a potential volume range of $0.5\text{--}4 \times 10^6 \text{ m}^3$. We were also concerned that because of the deep channel, the breadth of our simulated PF deposits could be too small, particularly if early deposits filled the channel to cause subsequent overbank PF flowage and deposits of broad lateral extent. Therefore we estimated an “overbank PF inundation zone”, by using an arbitrary A coefficient of 0.15, volume of $4 \times 10^6 \text{ m}^3$, and an arbitrary B coefficient ~ 100 , sufficient to enable the simulation to run out fully to distal areas. Thus our philosophy was to use our initial hazard zones to indicate mainly the *runout* potential for PFs of a specified volume, but to use the overbank PF zone to conservatively indicate the potential *breadth* of future PF deposits. We also estimated ash-cloud surge limits, which extended beyond the overbank PF zone, and are discussed below. Soon after our maps were delivered to Indonesia, several large block-and-ash PFs occurred as well as a number of smaller ones. On 14 June the largest PFs occurred and reached distances of $\sim 6 \text{ km}$ from the summit in the Gendol valley, damaged many buildings in Kaliadem/Bebeng, and killed two persons in a bunker near Kaliadem. Figure 5 shows our simulations, which were carried out on a 1995 DEM (C. Gerstenecker, unpublished data), superposed partly over a satellite image showing a PF on 16 June 2006 (Liew et al. 2008). The actual June 2006 deposits are shown in blue on Fig. 5, representing a cumulative deposit volume of $\sim 5.4 \times 10^6 \text{ m}^3$ (unpublished data, Merapi Volcano Observatory). The actual basal avalanche deposits were restricted to the main river channel, but overbank deposits spread onto interfluvies 3.2–5 km from the source and some were distributed into adjacent valleys (Gertisser and Charbonnier 2007). The boundary of actual deposits match rather well with the simulated overbank PF inundation zone, whereas the maximum runout is consistent

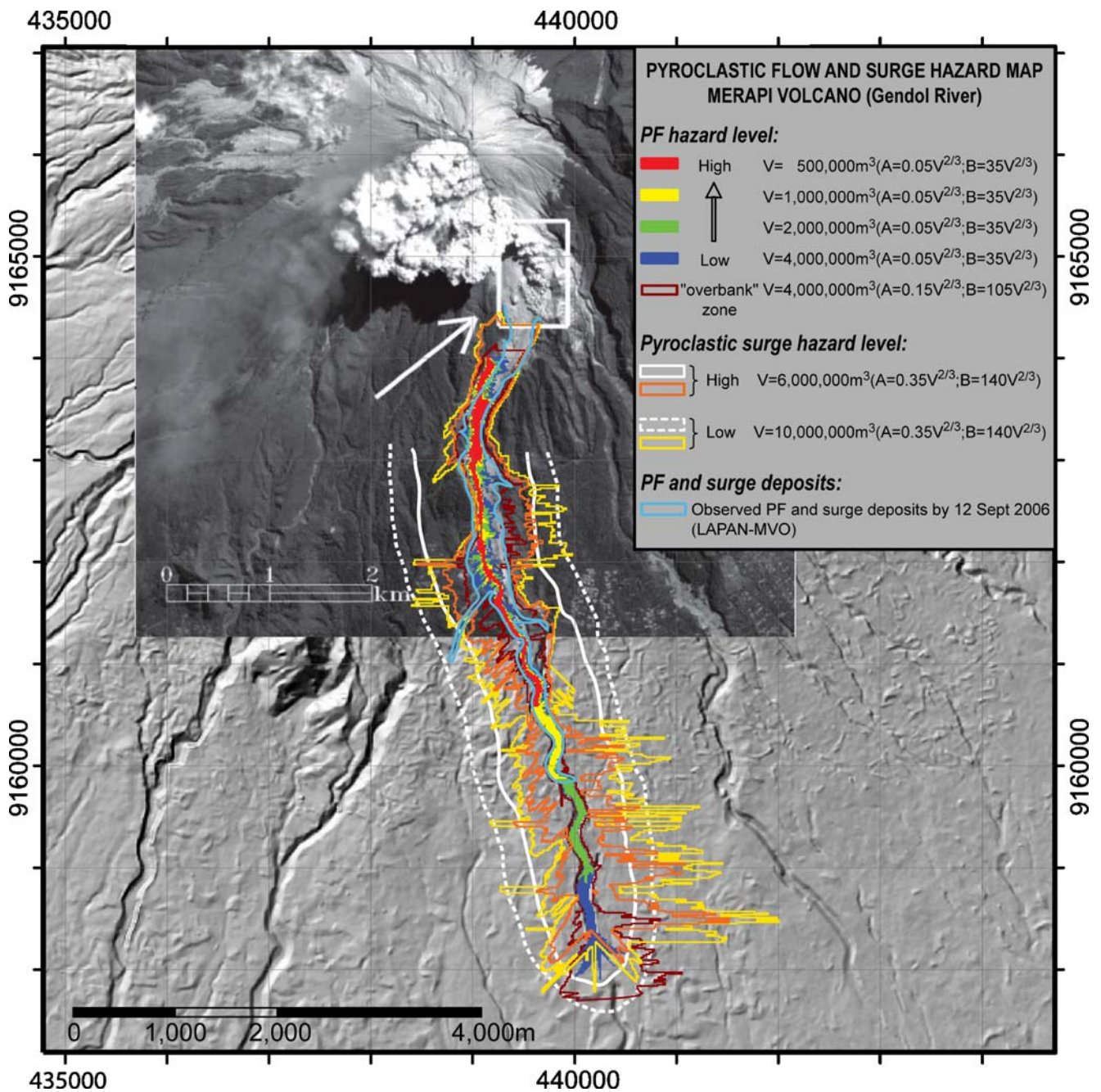


Fig. 5 Simulated inundations of block-and-ash PFs of selected volume for the Gendol River drainage, Merapi, to aid risk assessment in the volcanic crisis of June–July 2006. Parameters used were, $A=0.05 V^{2/3}$, $B=35 V^{2/3}$. PF hazard levels were graded from high to low, representing a potential volume range of $0.5\text{--}4 \times 10^6 \text{ m}^3$. An “over-bank PF inundation zone” was estimated by using an A coefficient of 0.15, volume of $4 \times 10^6 \text{ m}^3$, and B coefficient sufficient to enable full potential runoff; this zone was designed to encompass overflows if the channel prescribed by the DEM became sequentially filled. Surge limits were estimated using two methods. From Fig. 6, surge limits indicate distances from main channel, $\sim 700 \text{ m}$ (white dashed line,

relatively low hazard; 90% confidence level), and $\sim 500 \text{ m}$ (solid white line, high hazard; 50% confidence level). Surge limits were also determined by PFz methods using arbitrary parameters that yielded, on average in distal reaches, the empirical surge limits at 90% and 50% confidence levels. The two methods gave similar results where valley topography was normal, but results differed where local high ground adjacent to the channel restricted lateral runoff of surges as calculated by PFz. Map simulations superposed over satellite image showing PF on 16 June 2006 (in box; Liew et al. 2008; copyright CRISP, reproduced with permission). Actual deposits from June 2006 shown in blue

with the simulation for $V=1 \times 10^6 \text{ m}^3$; this volume is also a good estimate of the largest 14 June events.

As implied above, the use of the standard parameters alone may not be sufficiently conservative for hazards zonation, as the data could reflect a potential bias from deeply channeled topography on small-volume events, and the parameters do not encompass the effects of overspilling due to infilling of the channels, or uncertainties on the adequacy of the digital topography. Therefore we recommend that for practical hazards assessments, several inundation maps should be considered, using several coefficients of A , such as 0.05 and 0.1, to establish anticipated PF runouts, and a larger coefficient such as 0.15, as used for Merapi in conjunction with a conservatively large flow volume, to simulate the potential lateral breadth of dangerous overbank PFs. In the latter case the B parameter must be adjusted to yield the desired runout. This approach treats broadly the hazards implications of both runout and valley inundation breadth, to anticipate potential impacts on local populated areas. Calibrations of trial PFz maps with local PF deposits at the volcanoes of interest may also increase confidence in parameter selection.

Pyroclastic surges

Typically there are two main processes in dome-collapse pyroclastic flows, a basal “avalanche” and an overlying and a partly independent and possibly decoupled ash-cloud surge (Cas and Wright 1987; Fisher 1995; Fujii and Nakada 1999; Bourdier and Abdurachman 2001). In some cases with gas-pressurized domes, such pyroclastic surges can be

initiated very near the collapse source. Pyroclastic surges cause immediate scorching and destruction, and it is essential to include consideration of both pyroclastic flow and pyroclastic surge processes in the development of hazard maps. Surges can travel beyond the limits of the basal avalanche, thus in principle all PF zones should be encompassed within the envelope of a surge zone. We have approached this issue in several ways, by empirically examining the limits of pyroclastic surges associated with recent PFs, by developing an approach using *LAHARZ/PFz* methods, and by using a physics-based model to estimate the surge runout.

Figure 6 depicts the lateral extents of ash-cloud surge deposits or scorch limits for historical block-and-ash flows on the lower flanks of Merapi and Unzen volcanoes, as measured from the principal drainage channels (Voight et al. 2000a; Bourdier and Abdurachman 2001; Nakada and Fujii 1993; Yamamoto et al. 1993). The data suggest that for the typical channel morphology and physical character of the Merapi and Unzen flows (volume, gas content, etc.), ash-cloud surges could extend as far as one km laterally from the channel, and about one km in front of the PF snout. A more typical lateral value is about 300 m, and statistics suggest a predicted lateral limit of about 700 m with 90% confidence level, and about 500 m at 50% confidence level (Fig. 6). We used this information to augment our PFz maps generated in response to the Merapi eruption crisis in 2006 (Fig. 5).

We also developed another procedure for rapid estimation of surge limits, by simply using the standard *LAHARZ/PFz* approach, but with arbitrary large volumes and parameters adjusted such that the calculated lateral surge limits are similar on average to those surges observed historically (Figs. 5 and 6). However, rather than simply assuming a uniform constant-width lateral surge limit, this approach takes local topography into some consideration. Thus in some locations where topography is steep on one side of the valley, the lateral surge limits can be narrow on that side, but be more extensive on the other valley side where topography has low relief. Figure 5 illustrates the point. In the Merapi hazards assessment work, but not illustrated on Fig. 5, we also treated potentially accentuated surge runouts at channel bends in a qualitative manner.

Thus for the Merapi 2006 crisis we estimated potential ash-cloud surge limits using the two methods described above (Fig. 5). The map pattern shows two bands, each equidistant at 500 or 700 m from the channel, representing empirical 50% and 90% confidence levels on lateral surge limits. Surge limits were also estimated by PFz methods using arbitrary parameters that yielded, on average in distal reaches, the empirical surge limits at these same confidence levels. The differences in detail in the distal area largely reflect minor differences in real vs. idealized topography,

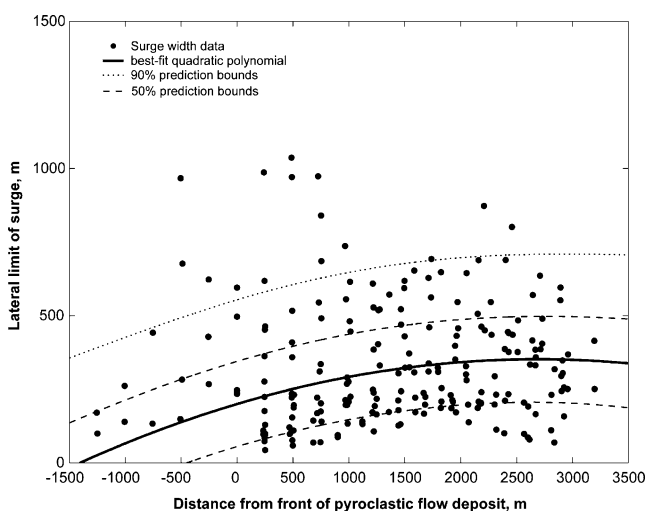


Fig. 6 Lateral extent of ash-cloud surge from main channel as a function of position relative to PF deposit front, at Merapi and Unzen volcanoes. Data sources noted in text

and the irregular edges reflect grid-cell computational aspects. The edges remain unsmoothed in this figure. The two methods gave roughly similar results where valley topography was normal, but results differed where local high ground adjacent to the channel restricted the surge lateral runout as calculated by *PFz*. In the actual block-and-ash flow events of June 2006, deposits from a hot ($>165^{\circ}\text{C}$) dilute ash-cloud surge were deposited on the valley margins, as much as 300 m from the channel (Gertisser and Charbonnier 2007). The observed 300 m lateral limit for the ash-cloud surge is typical for Merapi (Fig. 6), so surge deposits were well contained with respect to the conservative boundaries used in Fig. 5. The surge deposits were influenced by local topography, so that the surge limits suggested by *PFz* methods were somewhat more accurate than the bands drawn at constant distance from channel. On the other hand, at two locations, due to their ability to be re-channelized into adjacent river valleys oblique to the main basal avalanche flow direction, narrow re-channelized overbank flows extended beyond the PF hazard zones but were enclosed within the surge hazard zone (Fig. 5).

A pyroclastic surge can also be modeled following the approach of Bursik and Woods (1996) and Wadge et al. (1998), using a one-dimensional hydraulic balance of sedimentation of clasts and entrainment of air away from the modeled PF basal avalanche source. The idealized ash-cloud surge is assumed to flow normal or obliquely to the avalanche track, along a series of 1D flow paths defined by the DEM and broken into segments of constant slope and arbitrary length. A series of starting points for 1D surge calculations are selected along the PF channel (for procedural details see Wadge et al. 1998), or arbitrarily specified within the *PFz* inundation limits. An initial mass flux for the surge is specified (e.g., proportional to assumed PF volume). The surge is then assumed to move laterally from each starting point, while entraining air and sediment particles until the bulk density of the surge falls below that of ambient air, and lift-off occurs. This defines the surge deposit limit from each starting point. The connected deposit limits from a series of starting points thus give an estimate of the possible area that may be inundated by ash-cloud surges on each side of the PF.

The approach has been used on Montserrat for hazards assessments (Wadge et al. 1998; unpublished data). A surge limit produced by this method is illustrated in Fig. 4 (pale blue line, representing the estimated limit of surge for a $20 \times 10^6 \text{ m}^3$ dome collapse). A complicating aspect of this approach is that separate ash-cloud surge deposit limits can be established for each assumed PF volume, and thus “nested” surge deposit limits can be generated, with surge limits for smaller events fitting inside the limits for successively larger events. Plotting all surge limits calcu-

lated in this manner can result in an overly complicated map display. In the Montserrat case, the surge limits used and displayed for hazard and risk assessment purposes referred only to the vulnerable, populated western region (shown in pink on Fig. 4), and to selected large PF volumes necessary to reach this region. We mapped surge deposit limits only for the largest credible PF volumes.

Additionally, the surge *deposit* limits are not necessarily synonymous with surge *impact* limits, because scorching or searing can occur tens to hundreds of meters beyond the margin of surge deposits. For instance, observations at Merapi (Voight et al. 2000a; Aburachman et al. 2000; Shelley and Voight 1995; Kelfoun et al. 2000) and Montserrat (Loughlin et al. 2002a, b) show that a single zone beyond the surge deposit could be extensive and potentially fatal. This factor should be taken into account if surge deposit-limit maps are used as the basis for hazard maps.

Finally, we emphasize that caution is necessary in defining prospective surge deposit or surge impact limits. Some pyroclastic surges can develop in unexpected ways, such as the pyroclastic flow and surge event of 22 November 2004 at Merapi (Voight et al. 2000b; Abdurachman et al. 2000), and the dome collapse of 25 June 1997 on Montserrat (Fig. 3a; Loughlin et al. 2002a, b). These were not typical ash-cloud surges, but involved dispersal of large surge masses from initiation zones high on the volcano flanks, resulting in unusually broad swaths of destruction.

Discussion

The equations $A=(0.05 \text{ to } 0.1) V^{2/3}$, $B=(35 \text{ to } 40) V^{2/3}$ yield an objective, reproducible means to predict cross sectional (A) and planimetric (B) areas inundated by block-and-ash pyroclastic flows of various volumes (V). By comparison, the analogous predictive equations for lahars are $A=(0.05) V^{2/3}$, $B=(200) V^{2/3}$ (Iverson et al. 1998), and for rock avalanches, $A=(0.2) V^{2/3}$, $B=(20) V^{2/3}$ (Griswold and Iverson 2006). The similarity of equations implies that pyroclastic flows obey scaling rules similar to those for lahars and rock avalanches. The difference in proportionality coefficients (e.g., 35 or 40 vs. 200) indicates that pyroclastic flows of a given volume typically inundate areas that are five to six times smaller than lahars, and two times larger than rock avalanches. The difference is almost certainly related to the flow and friction reduction mechanisms of the different flowage types, and other factors such as scale. In lahars, high mobility is facilitated by solid–water interactions, the presence of liquefied debris with strong influence of pore-water pressures, and sluggish compaction dewatering and pore-water pressure dissipation (Iverson 1997; Major 1996). Pyroclastic flows are also influenced by solid–fluid interactions, but in this case the

fluid is juvenile gas, released into the flowing mixture by fragmentation of gas-charged vesicular lava clasts (Druitt 1998). Due to the low viscosity of gas, the fluid pressure in pyroclastic flows can dissipate much more rapidly than in lahars. In contrast, solid–fluid interactions are mostly absent or poorly developed in rock avalanches. These factors mainly account for the differences in mobility of these three flowage types, implied by their respective proportionality coefficients.

Several issues arise when applying this methodology and interpreting the results, and we emphasize some of the limitations here. Although the method is objective and reproducible, any PF inundation zone so computed should be considered as an approximate guide for hazards only, due to uncertainties in average coefficients with respect to individual PFs (which can vary in character), the variance of DEM details from actual topography, the indeterminacy of future collapse volumes, and uncertainty on the style and mode of evolution of future dome collapses. The gradational nested inundation maps based on a range of specified volumes can accommodate to some degree these types of uncertainty. Our comparisons of model inundation maps to actual recent PF deposits on Montserrat and Merapi gives some grounds for confidence, but substantial variation is allowed by the parameter confidence interval. For Montserrat we mainly used the A coefficient of 0.1 for these comparisons. Because of the substantial variation of valley slopes and topographies associated with the specific data, there was not a necessary guarantee of a good match between calculated inundation zones and specific deposit maps, and so the obtained good fit was reassuring. However, for our risk assessments at Montserrat involving potential *future* events, we also developed inundation maps using 0.05 as the parameter for the A calculation, which yielded results more conservative with respect to PF runout, although not to inundation breadth. The implications of these assumptions were then judged in relation to potential hazards affecting local populated areas.

A related complication is that many pyroclastic events occur in pulses, over tens of minutes or hours, and a question is whether to treat individual pulse volumes separately, or just the cumulative volume of the event. In general we have considered the full volume, inasmuch as individual pulse volumes are seldom recorded. Our opinion is that the cumulative volume should be used in most instances, because in a series of events the earlier events can cause infilling of channels and thus change topography, and the resulting deposit characteristics of the series of events will more closely reflect their full volume.

The PFz model does not explicitly consider dynamics aspects, which can be very important. Runup algorithms could be added (Iverson et al. 1998), but this would add undesirable complexity to the procedure and still not fully

resolve the issues. We have considered dynamics aspects primarily by use of alternative technologies, using the PFz maps to constrain dynamic parameters. The irregular “ragged” appearance of some PFz maps, particularly in distal regions, may be disconcerting to interpreters or decision makers, and smoothing of these maps would normally be desirable before they are distributed (Iverson et al. 1998).

It is possible to rank hazard in relative terms, as a suite of hazard zones grading from high to low, instead of by reference to specific volumes. This was done in our PFz maps of Merapi, which were distributed to hazards managers in Indonesia. However, in some cases the use of specific PF volumes may be desired when quantitative consideration and emphasis is given to the potential volumes that could be released from a source area, and decision-makers are aware of these source volumes (this was the case for Montserrat hazard assessments in January 2007). A more quantitative interpretation could also include PF recurrence probabilities. The issue is complicated (Iverson et al. 1998), but such data may be locally available (Aspinall et al. 2002).

Local topography can change rapidly around erupting volcanoes, largely due to channel infilling by pyroclastic flows and lahars, and also due to alterations in the character and direction of lava dome growth that change hazard perspectives. Older topographic maps may then no longer be strictly valid, and DEMs may need to be updated frequently to keep hazards mapping current. Any inundation or hazard maps produced should be dated to note the time period of relevance, and updates made (if possible) as a dynamic situation evolves. Changes of dome growth that lead to concentrations of pyroclastic activity in certain drainages may warrant hazard zones of extended length and breadth in that drainage. Such changes can occur rapidly, even within an individual event, with multiple pyroclastic flows following in rapid succession. In such cases the base topography of the model can rapidly become obsolete, or at least incorrect in details that can importantly influence flowage and deposition. The use of nested inundation maps with variable flow volumes can capture some of this uncertainty, as can the use of adjusted parameters to capture overbank flowage and ash-cloud surge limits (Fig. 5).

Finally, although this paper has concentrated on a procedure to predict cross sectional and planimetric areas inundated by block-and-ash pyroclastic flows, we believe that the general approach will likely also prove useful for pyroclastic flows generated by fountain collapse. The parameter values will not be the same, however, and a suitable database is not yet available to define them. Pyroclastic flows from fountain collapse of a given volume can be more mobile than those derived from dome collapse. Sites subjected to fountain collapse may also require examination of base surges as well as ash-cloud surges.

Conclusions

Our results support the following conclusions:

1. The semi-empirical equations $A=(0.05 \text{ to } 0.1) V^{2/3}$, $B=(35 \text{ to } 40) V^{2/3}$ yield an objective, reproducible means to predict cross sectional (A) and planimetric (B) areas inundated by block-and-ash pyroclastic flows of various volumes (V). The proportionality coefficients suggest that pyroclastic flows of a given volume typically inundate areas that are five or six times smaller than lahars, and two times larger than rock avalanches.
2. The delineation of such PF hazard zones can be accomplished most easily by using the *LAHARZ* suite of GIS programs (Schilling 1998; Iverson et al. 1998).
3. Nested inundation maps for various volumes effectively depict the decrease in hazards with distance from the volcano and lateral distance from the valley thalweg, and provide a measure of the distribution of the PF mass and deposition level above the valley floor. Such nested hazard maps have proven useful for mitigation responses.
4. Although the method is objective and reproducible, any specific PF inundation zone so computed should be considered as an approximate guide for hazards only, due to uncertainties in average coefficients with respect to individual PFs (which can vary in character), DEM details and currency, and uncertainty of future collapse volumes. Our comparisons of PFz inundation maps to actual recent PF deposits give some grounds for confidence, but substantial variation is allowed by the parameter confidence interval. The gradational nested inundation maps partly accommodate these types of uncertainty, and thus can assist in practical hazards situations where neither the volumes of dangerous future events or their dynamic attributes can be predicted with confidence.
5. The standard parameters do not encompass the uncertainty on the adequacy of the digital topography or the possibility of channel infilling leading to overspilling of PFs. Thus we recommend that for practical hazards assessments, several inundation maps should be considered, using several coefficients of A , such as 0.05 and/or 0.1, to establish anticipated PF runouts, and also a larger coefficient such as 0.15, as used for Merapi in conjunction with a conservatively large flow volume, to simulate the potential lateral breadth of dangerous overbank PFs. In the latter case the B parameter must be adjusted to yield the desired runout. This approach treats broadly the hazards implications of both runout distance and valley inundation breadth.
6. The base method does not explicitly consider either flow path dynamics or ash-cloud surges which com-

monly accompany block-and-ash flows. However, we have presented methods to approach these issues. Some consideration of both aspects is highly desirable for a complete hazards assessment. In principle, all PF inundation zones should be depicted within a pyroclastic surge inundation zone.

7. The above approach can be used alone, or in combination with some flow dynamics codes, which themselves are commonly limited due to their high sensitivity to dynamic parameters that normally are poorly constrained. By varying dynamic parameters to yield deposit areas that match the semi-empirical PFz inundation zones, one can gain perspective into dynamics of channel bend run-up or overflows, prior to the accumulation of debris at the depositional site.
8. This paper has concentrated on a procedure to predict cross sectional and planimetric areas inundated by block-and-ash pyroclastic flows and ash-cloud surges, but our belief is that the general approach will likely also prove useful for pyroclastic flows generated by fountain collapse. The parameter values will not be the same, however, and further work is needed to develop a suitable database and to test appropriate parameter values.
9. The method has been used to quickly and effectively supply PF hazard maps in two volcanic crises: Merapi 2006; and Montserrat 2006–2007.

Acknowledgments This work was supported by the National Science Foundation EAR-04-08709 to BV. A special motivation for these studies arose from BV's associations with Dick Janda and Harry Glicken; Janda and BV mapped PF and surge hazard zones at Galeras volcano in 1989, and Glicken, with the Kraffts, was killed by an ash-cloud surge at Unzen in 1991. Our research follows the seminal approach of R.M. Iverson, S.P. Schilling, and J.W. Vallance in regard to delineation of lahar-inundation zones. We thank others at USGS for comments on our generation of maps for the Merapi crisis, including C. Newhall, J. Pallister, W. Scott, J.J. Major, and J. Griswold. With regard to Montserrat, we thank G. Wadge, R. Herd, and MVO staff for valuable discussions and updated DEM data. USGS internal reviews for this paper were kindly provided by J.J. Major, D. Dzurisin, W.E. Scott and R.M. Iverson. Reviews for the journal were contributed by A. Neri and S.C. Loughlin. We are grateful to all reviewers for numerous insightful comments that improved our paper. The opinions expressed in the paper are those of the authors alone.

References

- Abdurachman EK, Bourdier JL, Voight B (2000) Nuées ardentes of November 22, 1994 at Merapi Volcano, Indonesia. *J Volcanol Geotherm Res* 100:345–361
- Aspinall WP, Loughlin SC, Michael FV, Miller AD, Norton GE, Rowley KC, Sparks RSJ, Young SR (2002) The Montserrat Volcano Observatory: its evolution, role, and activities. In: Druitt TH, Kokelaar BP (eds) *The eruption of Soufrière Hills volcano, Montserrat, from 1995 to 1999*. Geol Soc London, *Memoirs*, vol. 21. Geological Society, London, pp 71–91

- Bourdier JL, Abdurachman EK (2001) Decoupling of small-volume pyroclastic flows and related hazards at Merapi volcano, Indonesia. *Bull Volcanol* 63:309–325 doi:10.1007/s004450100133
- Bursik MI, Woods AW (1996) The dynamics and thermodynamics of large ash clouds. *Bull Volcanol* 58:175–193
- Calder ES, Cole PD, Dade WB, Druitt TH, Hoblitt RP, Huppert HE, Ritchie L, Sparks RSJ, Young SR (1999) Mobility of pyroclastic flows and surges at the Soufrière Hills Volcano, Montserrat. *Geophys Res Lett* 26:537–540
- Calder ES, Luckett R, Sparks RSJ, Voight B (2002) Mechanisms of lava dome instability and generation of rockfalls and pyroclastic flows at Soufrière Hills Volcano, Montserrat. In: Druitt TH, Kokelaar BP (eds) The eruption of Soufrière Hills volcano, Montserrat, from 1995 to 1999. *Geol Soc London, Memoirs*, vol. 21. Geological Society, London, pp 173–190
- Cas RAF, Wright JV (1987) Volcanic successions: modern and ancient. Allen & Unwin, London, pp 1–528
- Cole PD, Calder ES, Sparks RSJ, Clarke AB, Druitt TH, Young SR, Herd RA, Harford CL, Norton GE (2002) Deposits from dome-collapse and fountain-collapse pyroclastic flows at Soufrière Hills Volcano, Montserrat. In: Druitt TH, Kokelaar BP (eds) The eruption of Soufrière Hills volcano, Montserrat, from 1995 to 1999. *Geol Soc London, Memoirs*, vol. 21. Geological Society, London, pp 231–262
- Crandell DR, Booth B, Kusumadinata K, Shimozuru D, Walker GPL, Westercamp D (1984) Source-book for volcanic-hazards zonation. *Nat Hazards* 4:1–97, UNESCO, Paris
- Denlinger RP, Iverson RM (2001) Flow of variably fluidized granular masses across three-dimensional terrain 2. Numerical predictions and experimental tests. *J Geophys Res* 106(B1):553–566
- Druitt TH (1998) Pyroclastic density currents. In: Gilbert JS, Sparks RSJ (eds) The physics of explosive volcanic eruptions. *Geol Soc Special Pub* 145. Geological Society, London, pp 145–182
- Esposti Ongaro T, Cavazzoni C, Erbacci G, Neri A, Salvetti MV (2007) A parallel multiphase flow code for the 3D simulation of explosive volcanic eruptions. *Parallel Computing* 33:541–560 doi:10.1016/j.parco.2007.04.003
- Esposti Ongaro T, Neri A, Clarke A, Voight B, Widiwijayanti C (2008) Fluid dynamics of the 1997 Boxing Day volcanic blast on Montserrat, West Indies. *J Geophys Res* 113:B03211 doi:10.1029/2006JB004898
- Fisher RV (1995) Decoupling of pyroclastic currents: hazards assessment. *J Volcanol Geotherm Res* 66:257–263
- Fujii T, Nakada S (1999) The 15 September 1991 pyroclastic flows at Unzen Volcano (Japan): a flow model for associated ash-cloud surges. *J Volcanol Geotherm Res* 89:159–172
- Gertisser R, Charbonnier SJ (2007) Block-and-ash flow deposits of the 2006 eruption of Merapi Volcano, Java, Indonesia. In: Abstracts Volume, Fifth Conference, Cities On Volcanoes, IAVCEI, Shimabara, Japan, Abstract 11-P-29
- Griswold J, Iverson RM (2006) Statistical indices of the relative mobilities of debris flows, rock avalanches, and lahars. *Eos Trans AGU* 87(52) Fall Meet Suppl Abstract H53D-0660
- Iverson RM (1997) The physics of debris flows. *Rev Geophys* 35:245–296
- Iverson RM, Schilling SP, Vallance JW (1998) Objective delineation of lahar-inundation hazard zones. *Geol Soc Amer Bull* 110:972–984
- Kelfoun K, Legros F, Gourgaud A (2000) A statistical study of trees damaged by the 22 November 1994 eruption of Merapi volcano (Java, Indonesia): relationships between ash-cloud surges and block-and-ash flows. *J Volcanol Geotherm Res* 100:379–393
- Kokelaar BP (2002) Setting, chronology and consequences of the eruption of Soufrière Hills Volcano, Montserrat. In: Druitt TH, Kokelaar BP (eds) The eruption of Soufrière Hills volcano, Montserrat, from 1995 to 1999. *Geol Soc London, Memoirs*, vol. 21. Geological Society, London, pp 1–43
- Liew SC, Thouret J-C, Gupta A, Kwok LK (2008) First satellite image of a moving pyroclastic flow. *Eos Trans AGU* 89(22):202
- Loughlin SC, Calder ES, Clarke A, Cole PD, Luckett R, Mangan MT, Pyle DM, Sparks RSJ, Voight B, Watts RB (2002a) Pyroclastic flows and surges generated by the 25 June 1997 dome collapse, Soufrière Hills Volcano, Montserrat. In: Druitt TH, Kokelaar BP (eds) The eruption of Soufrière Hills volcano, Montserrat, from 1995 to 1999. *Geol Soc London, Memoirs*, vol. 21. Geological Society, London, pp 191–209
- Loughlin SC, Baxter PJ, Aspinall WA, Darroux B, Harford CL, Miller AD (2002b) Eyewitness accounts of the 25 June 1997 pyroclastic flows and surges at Soufrière Hills Volcano, Montserrat, and implications for disaster mitigation. In: Druitt TH, Kokelaar BP (eds) The eruption of Soufrière Hills volcano, Montserrat, from 1995 to 1999. *Geol Soc London, Memoirs*, vol. 21. Geological Society, London, pp 211–230
- Major JJ (1996) Experimental studies of deposition by debris flows: Process, characteristics of deposits, and effects of pore-fluid pressure. Ph.D. dissertation, Seattle, Univ Washington, pp 1–341
- Major JJ, Schilling SP, Pullinger CR, Escobar CD (2004) Debris-flow hazards at San Salvador, San Vicente, and San Miguel volcanoes, El Salvador. *Geol Soc America Spec Pap* 375:89–108
- Malin MC, Sheridan MF (1982) Computer-assisted mapping of pyroclastic surges. *Science* 217:637–640
- Nakada S, Fujii T (1993) Preliminary report on volcanic activity at Unzen Volcano, November 1990–November 1991: Dacite lava domes and pyroclastic flows. *J Volcanol Geotherm Res* 54:319–333
- Norton GE, Watts RB, Voight B, Mattioli GS, Herd RA, Young SR, Devine GE, Aspinall WP, Bonadonna C, Baptie BJ, Edmonds M, Jolly AD, Loughlin SC, Luckett R, Sparks RSJ (2002) Pyroclastic flow and explosive activity at Soufrière Hills Volcano, Montserrat, during a period of virtually no magma extrusion (March 1998 to November 1999). In: Druitt TH, Kokelaar BP (eds) The eruption of Soufrière Hills volcano, Montserrat, from 1995 to 1999. *Geol Soc London, Memoirs*, vol. 21. Geological Society, London, pp 467–481
- Patra AK, Bauer AC, Nichita CC, Pitman EB, Sheridan MF, Bursik M, Rupp B, Webber A, Stinton A, Namikawa L, Renschler C (2005) Parallel adaptive simulation of dry avalanches over natural terrain. *J Volcanol Geotherm Res* 139:1–21
- Ratdomopurbo A (2007) Precursory data of the 2006 Eruption of Mt. Merapi. In: Abstracts Volume, Fifth Conference, Cities On Volcanoes, IAVCEI, Shimabara, Japan, Abstract 12-O-04
- Saucedo R, Macías JL, Bursik MI, Mora JC, Gavilanes JC, Cortes A (2002) Emplacement of pyroclastic flows during the 1998–1999 eruption of Volcán de Colima, México. *J Volcanol Geotherm Res* 117:129–153
- Saucedo R, Macías JL, Bursik MI (2004) Pyroclastic flow deposits of the 1991 eruption of Volcán de Colima, México. *Bull Volcanol* 66:291–306
- Saucedo R, Macías JL, Sheridan MF, Bursik MI, Komorowski JC (2005) Modeling of pyroclastic flows of Colima Volcano, Mexico: implications for hazard assessment. *J Volcanol Geotherm Res* 139:103–115
- Schilling SP (1998) LAHARZ: GIS programs for automated mapping of lahar-inundation zones. *US Geol. Survey, Open-file Report* 98–638
- Schwarzkopf LM, Schmincke HU (2000) The July 1998 eruptions of Merapi volcano: stratigraphy and volumes of the block-and-ash flow deposits. In: Proc. 2nd Merapi-Galeras Workshop ‘Decade Volcanoes under investigation’. Sonderband DGG-Mitteilungen IV/2000, pp 7–10
- Shelley I, Voight B (1995) Medical effects of nuées ardentes eruptions: The November 1994 eruption at Merapi Volcano, Indonesia. In: Proc Merapi Decade Volcano Workshop, UNESCO/Volcanol Survey Indonesia, Yogyakarta, pp 9–9
- Sparks RSJ, Barclay J, Calder ES, Herd RA, Komorowski J-C, Luckett R, Norton GE, Ritchie LJ, Voight B, Woods AW (2002) Generation of

- a debris avalanche and violent pyroclastic density current on 26 December (Boxing Day) 1997 at Soufrière Hills Volcano, Montserrat. In: Druitt TH, Kokelaar BP (eds) The eruption of Soufrière Hills volcano, Montserrat, from 1995 to 1999. Geol Soc London, Memoirs, vol. 21. Geological Society, London, pp 409–434
- Voight B, Constantine EK, Siswoidjyo S, Torley R (2000a) Historical activity at Merapi Volcano, Java, Indonesia, 1768–1998. *J Volcanol Geotherm Res* 100:69–138
- Voight B, Young KD, Hidayat D, Subandrio, Purbawinata MA, Ratdomopurbo A, Suharna, Panut, Sayudi DS, LaHusen R, Marso J, Murray TL, Dejean M, Iguchi M, Ishihara K (2000b) Deformation and seismic precursors to dome-collapse and fountain-collapse nuées ardentes at Merapi Volcano, Java, Indonesia 1994–1998. *J Volcanol Geotherm Res* 100:261–287
- Wadge G, Jackson P, Bower SM, Woods AW, Calder E (1998) Computer simulations of proclastic flows from dome collapse. *Geophys Res Lett* 25(19):3677–3680
- Widiwijayanti C, Voight B, Hidayat D, Patra A, Pitman EB (2004) Validation of TITAN2D flow model code for pyroclastic flows and debris avalanches at Soufrière Hills Volcano, Montserrat, BWI, *Eos Trans AGU* 85(47) Fall Meet Suppl Abstract V43B-1428
- Widiwijayanti C, Hidayat D, Voight B, Patra A, Pitman EB (2006) Modelling pyroclastic Flows with TITAN2D. In: Abstracts Volume, Fourth Conference, Cities On Volcanoes, IAVCEI, Quito, Ecuador, Abstract 4.48.
- Yamamoto T, Takarada S, Suto S (1993) Pyroclastic flows from the 1991 eruption of Unzen volcano, Japan. *Bull Volcanol* 55:166–175